

# Strongly nonlinear convection in binary fluids: minimal model using symmetry decomposed modes

St. Hollinger, M. Lücke

Institut für Theoretische Physik, Universität des Saarlandes, Postfach 151150, D-66041 Saarbrücken, Germany

Received: 12 December 1996

**Abstract.** Spatially extended stationary and traveling states in the strongly nonlinear regime of convection in layers of binary fluid mixtures heated from below are described by a few-mode-model. It is derived from the proper hydrodynamic balance equations including experimentally relevant boundary conditions with a non-standard Galerkin approximation that uses numerically obtained, symmetry decomposed modes. Properties of the model are elucidated and compared with full numerical solutions of the field equations.

**PACS:** 47.20.-k; 47.10.+g; 03.40.Gc

## I. Introduction

Convection in binary miscible fluids like, e. g., ethanol-water is a paradigmatic system for studying instabilities, bifurcations, complex spatio-temporal behaviour, and turbulence. Furthermore, it is sufficiently simple to allow for controlled experiments and the governing field equations are well known. So recently a lot of research activities [1–13] have been directed towards investigating the enormous variety of pattern forming behaviour in this system. The richness of spatio-temporal phenomena in binary fluid mixtures stems from a feed-back loop between the fields of velocity, concentration, and temperature. Let us start with the velocity field: The convective flow is driven by the buoyancy force field which itself is determined by variations of the temperature and of the concentration field. The latter are on the one hand generated via the thermodiffusive Soret effect by temperature gradients and on the other hand they are reduced by concentration diffusion and by mixing through the convective flow. Since these changes influence the buoyancy which drives the flow the feed back loop is closed.

In this article we concentrate on spatially extended convection states of straight parallel rolls that occur either as a horizontally traveling wave (TW) or in the form of stationary “overturning” convection (SOC) rolls. In particular, we

derive a model which is able to describe also stable TWs in the strongly nonlinear regime and which goes beyond earlier approximations that are applicable only to the weakly nonlinear regime. We present and explore here the properties of a minimal Galerkin model that is based on a symmetry decomposition of numerically obtained fields. It reproduces the typical bifurcation scenario obtained from simulations and experiments.

For fluid parameters typically realized in mixtures of water and about 10 wt.% ethanol, an oscillatory, subcritical onset of convection is observed. It is connected by an unstable TW branch with a saddle-node bifurcation giving rise to stable, strongly nonlinear TW states. At a certain Rayleigh number, the phase velocity of these waves vanishes and the SOC branch of stable stationary states can be observed. Along the TW bifurcation branch which is shown in detail in Figs. 1 and 4 the concentration changes its structure from lateral homogeneity and vertically linear layering in the basic state over plateau-like distributions in fast TWs to boundary layer dominated, slowly traveling waves. The contrast between two adjacent TW rolls is strongly related to the phase velocity of the TW and it vanishes with this velocity. So, SOC rolls do not show such a concentration contrast. In SOC rolls adjacent rolls are mirror images of each other and they are separated from another and from the top and bottom plate only by thin boundary layers. The latter are a typical phenomenon for convection of weakly diffusing scalars. To capture this behaviour of the concentration field our model contains more degrees of freedom of the concentration field than of the velocity and of the temperature field.

Our article is organized as follows: The *second* section presents the system, the fields needed for its description, their governing equations with the explanation of the relevant fluid and control parameters. The *third* section shows which symmetries in TW and SOC convection occur and how they change at the bifurcations. Furthermore, a discussion of the symmetry decomposed balance equations and of their numerically found solutions is given. Out of this data we extract in the *fourth* section a basis for a non-standard Galerkin approximation. Its results are presented in bifurcation diagrams of different order parameters in comparison with the correct solutions of the system. We also discuss

predictions of our model concerning the dependence of the bifurcation topology on the strength of the Soret coupling.

## II. System

The fields needed for the description of straight parallel rolls in a horizontal fluid layer exposed to a vertical gravitational acceleration  $g$  are temperature  $T$ , concentration  $C$ , and velocity  $\mathbf{u} = (u, 0, w)$ . Here,  $u$  is the velocity field in the lateral  $x$ -direction and  $w$  is the velocity in the vertical  $z$ -direction. Fluid parameters are the Prandtl number  $\sigma = \nu/\kappa$ , the Lewis number  $L = D/\kappa$ , and the separation ratio  $\psi = -\beta k_T/(\alpha T_0)$ .  $\nu$  is the kinematic viscosity,  $\kappa$  the thermal diffusivity,  $D$  the diffusion coefficient,  $\alpha = -(1/\rho) (\partial\rho/\partial T)$  and  $\beta = -(1/\rho) (\partial\rho/\partial C)$  thermal and solutal expansion coefficients,  $\rho$  the fluid's density,  $k_T$  the thermodiffusion ratio, and  $T_0$  ( $C_0$ ) the mean temperature (concentration) in the system. We scale lengths by the height  $d$  of the fluid layer, times by the vertical thermal diffusion time  $d^2/\kappa$ , temperatures by the imposed vertical temperature difference  $\Delta T$ , and concentrations by  $\Delta T\alpha/\beta$ . Our control parameter is the Rayleigh number  $R = \alpha g d^3 \Delta T/(\nu\kappa)$ . Mostly we use the reduced Rayleigh number  $r = R/R_c^0$  where  $R_c^0$  denotes the critical Rayleigh number for the onset of convection in a pure fluid ( $R_c^0 = 1707.762$ ;  $R_c^0 \simeq 1747.28$  in our model).

We start with the hydrodynamic field equations in a nondimensional version using the scales defined above. They represent balances for momentum, heat, and concentration

$$\partial_t \mathbf{u} + \mathbf{u} \cdot \nabla \mathbf{u} = -\nabla p + \sigma \{ R [(T - T_0) + (C - C_0)] \mathbf{e}_z + \nabla^2 \mathbf{u} \} \quad (2.1a)$$

$$\partial_t T + \mathbf{u} \cdot \nabla T = \nabla^2 T \quad (2.1b)$$

$$\partial_t C + \mathbf{u} \cdot \nabla C = L \nabla^2 C - L \psi \nabla^2 T. \quad (2.1c)$$

Assuming an incompressible fluid — this is reasonable as long as the convective velocities in the fluid are small in comparison with the velocity of the sound — the density is constant and the continuity equation as the balance equation for the total mass leads to

$$\nabla \cdot \mathbf{u} = 0 \quad .$$

In (2.1), the temporal changes of a field are given by convective transport of that field on the left hand side of the equation. Apart from the advective rate of change the momentum (2.1a) changes by pressure gradients ( $-\nabla p$ ) and dissipative effects ( $\sigma \nabla^2 \mathbf{u}$ ). The gravitational acceleration acts as an external force ( $R [(T - T_0) + (C - C_0)] \mathbf{e}_z$ ) on the fluid. At that point, density fluctuations due to temperature and concentration fluctuations may not be ignored since they represent the driving of the system.

The heat balance (2.1b) takes advective ( $\mathbf{u} \cdot \nabla T$ ) and diffusive ( $\nabla^2 T$ ) transport into account. In the case of the concentration balance (2.1c), the cross coupling of the temperature to the concentration ( $-L\psi \nabla^2 T$ ) is a relevant effect. It is called thermodiffusion or Soret effect [1, 2]. For negative separation ratios  $\psi$ , it acts in such a way that temperature gradients induce antiparallel concentration gradients;

positive values of  $\psi$  lead to parallel ones. If the Soret coupling  $\psi$  vanishes, as it occurs in ethanol water mixtures of a concentration of 0 and 28 wt.%, the mixture behaves just like a pure fluid.

From these remarks, the stability behaviour may be inferred: For negative separation ratios, the unstable layering of the density is reduced, for positive ones it is increased compared with the situation in a pure fluid. Thus, mixtures with  $\psi < 0$  ( $\psi > 0$ ) have larger (smaller) critical Rayleigh numbers than the pure fluid. Below these threshold values, a motionless ( $\mathbf{u} \equiv 0$ ) state with the laterally homogeneous conductive profiles

$$T_{\text{cond}}(z) = T_0 - z$$

$$C_{\text{cond}}(z) = C_0 - \psi z$$

of temperature and concentration, respectively, is a stable solution of (2.1). Above threshold this solution becomes unstable to convection. It is convenient to use

$$\theta = T(x, z, t) - T_{\text{cond}}(z) \quad (2.2a)$$

$$c = C(x, z, t) - C_{\text{cond}}(z) \quad (2.2b)$$

as convective deviations of temperature and concentration from their conductive profiles for straight rolls in  $y$ -direction.

In this paper we discuss convective roll solutions of (2.1) which have a lateral wave number of  $k = \pi$  being close to the critical values around 3.116. These solutions are either stationary or they represent traveling waves. The latter are stationary in a frame comoving with the phase velocity  $v$  of the traveling wave relative to the laboratory frame. In the comoving frame ( $v \equiv 0$  for states being stationary in the laboratory frame), we introduce the streamfunction  $\Phi(x, z)$  which describes the incompressible twodimensional convective flow

$$\mathbf{u}(x, z) = (u(x, z), 0, w(x, z)) = (-\partial_z, 0, \partial_x)\Phi(x, z) \quad (2.3)$$

in the  $x-z$  plane perpendicular to the roll axes. The velocity field  $\mathbf{u}(x, z)$  (2.3) guarantees incompressibility,  $\nabla \cdot \mathbf{u} = 0$ , by construction.

The traveling and stationary states are solutions of the time independent field equations

$$\mathcal{J}(\Phi, \nabla^2 \Phi) = \sigma [R \partial_x (\theta + c) + \nabla^4 \Phi] \quad (2.4a)$$

$$\mathcal{J}(\Phi, \theta) = \partial_x \Phi + \nabla^2 \theta \quad (2.4b)$$

$$\mathcal{J}(\Phi, c) = \psi \partial_x \Phi + L \nabla^2 (c - \psi \theta) \quad (2.4c)$$

in the comoving frame. They can directly be deduced from (2.1). Herein, we used the Jacobian

$$\mathcal{J}(\Phi, f) := (\partial_x \Phi) \partial_z f - (\partial_z \Phi) \partial_x f \equiv (\mathbf{u} \cdot \nabla) f$$

to describe the convective nonlinearity.

The boundary conditions at  $z = \pm 1/2$  in the comoving frame are for all  $x$

$$\begin{aligned} \text{no slip} & \quad u = -\partial_z \Phi = -v \quad , \\ & \quad w = \partial_x \Phi = 0 \quad , \\ \text{perfectly heat conducting} & \quad \theta = 0 \quad , \text{ and} \\ \text{impermeable} & \quad \partial_z (c - \psi \theta) = 0 \quad . \end{aligned} \quad (2.5)$$

Numerical simulations [13] and a full scale Galerkin analysis with many trigonometric modes for the fields [15] have shown that the contribution from lateral Fourier modes higher than the first one in the velocity field is only in a range of 1% of the first one and that these higher velocity modes are unnecessary for reproducing the bifurcation topology and the peculiar structure of the concentration field, respectively. The analyses [13, 15] have also proved the irrelevance of a lateral meanflow in the lateral velocity field. Therefore, we start our approximations with the ansatz

$$\tilde{\Phi}(x, z) = \frac{w_{\max}}{k \mathcal{E}_1(0)} \sin kx \mathcal{E}_1(z) + vz =: \tilde{\Phi}(x, z) + vz \quad (2.6)$$

for the streamfunction. Here,  $\mathcal{E}_1(z)$  is the first even Chandrasekhar function [16],  $w_{\max}$  the maximal flow amplitude, and  $v$  the phase velocity of the traveling state. These two velocities are the only degrees of freedom of the velocity field. By the above ansatz for the streamfunction we fix the origin  $x = 0, z = 0$  of the coordinate system to a point of maximal upflow velocity.

### III. Symmetries

In this section we discuss symmetries of the fields in the coordinate system defined in the last section and we perform a symmetry decomposition of the fields and their balance equations. After this, we analyse the relative weight of contributions from different symmetries in the solutions of the field equations.

#### A. Decomposition

Nonlinear states of stationary convection (SOCs) have definite parity [13] under the operation  $x \rightarrow -x$ : positive parity for the fields  $w, \theta$ , and  $c$ , and a negative one for  $\tilde{\Phi}$  and  $u$ . Only the linear critical fields at the stationary bifurcation threshold have in addition definite vertical parity under the operation  $z \rightarrow -z$ : positive parity for the fields  $w, \tilde{\Phi}, \theta$ , and  $c$ , and a negative for  $u$ .

Traveling wave states with non vanishing phase velocity have no definite lateral parity. Only that TW just on the merging point  $r^*$  of the branches of SOC and TWs has, of course, the same symmetry as the stationary states. At the Hopf bifurcation out of the basic state, the linear critical fields have definite vertical parity, which is destroyed by the action of the convective nonlinearity in every nonlinear state.

The temperature and concentration fields are decomposed in four parts each, corresponding to the four different combinations of vertical and lateral parity

$$\theta = \theta^{++} + \theta^{+-} + \theta^{-+} + \theta^{--} \quad (3.1a)$$

$$c = c^{++} + c^{+-} + c^{-+} + c^{--} \quad (3.1b)$$

Here, the first (second) superscript denotes the parity in lateral (vertical) direction. The symmetries themselves will be labelled by  $\mathcal{S}^{\pm\pm}$  in the same way. A symmetry decomposition of the velocity field or of the streamfunction is not necessary, since their spatial variation is fixed by (2.4). The

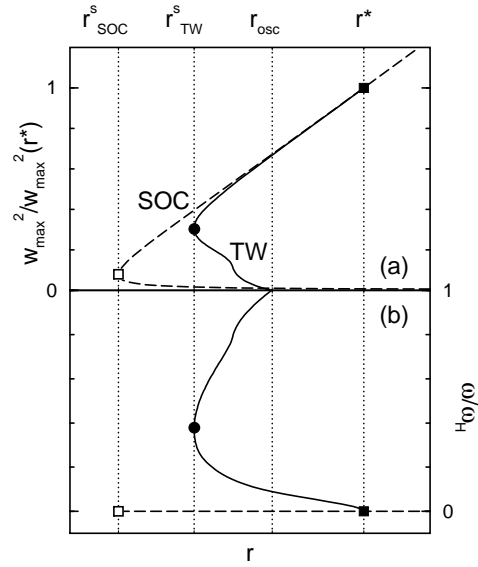


**Fig. 1.** Bifurcation diagrams of reduced convection flow intensity **a** and frequency **b** in TW (solid lines) and SOC (dashed lines) solutions in a binary mixture with  $\psi = -0.25$ ,  $L = 0.01$  and  $\sigma = 10$

decomposition of the balance equation for the concentration (2.3c) yields the following four equations after inserting the streamfunction  $\tilde{\Phi}$  (2.4) into (2.3c)

$$\mathcal{J}(\tilde{\Phi}, c^{+-}) - v \partial_x c^{+-} = L \nabla^2 (c^{+-} - \psi \theta^{+-}) + \psi \partial_x \tilde{\Phi} \quad (3.2a)$$

$$\mathcal{J}(\tilde{\Phi}, c^{++}) - v \partial_x c^{++} = L \nabla^2 (c^{++} - \psi \theta^{++}) \quad (3.2b)$$

$$\mathcal{J}(\tilde{\Phi}, c^{--}) - v \partial_x c^{--} = L \nabla^2 (c^{--} - \psi \theta^{--}) \quad (3.2c)$$

$$\mathcal{J}(\tilde{\Phi}, c^{-+}) - v \partial_x c^{-+} = L \nabla^2 (c^{-+} - \psi \theta^{-+}) \quad (3.2d)$$

The decomposition of the heat balance equation (2.3b) can be performed in a completely analogous way. Using the ansatz (2.4) for the streamfunction the momentum balance can be split into two parts: one for the symmetry  $\mathcal{S}^{++}$  and one for  $\mathcal{S}^{-+}$

$$-v \partial_x \nabla^2 \tilde{\Phi} = R \sigma \partial_x (\theta^{-+} + c^{-+}) \quad (3.3a)$$

$$0 = R \partial_x (\theta^{++} + c^{++}) + \nabla^4 \tilde{\Phi} \quad (3.3b)$$

All together, eight partial differential equations must be solved for the temperature and concentration fields. The two degrees of freedom of the velocity field,  $w_{\max}$  and  $v$ , are determined by algebraic equations which result from projecting (3.3) onto the fixed spatial modes of the streamfunction (2.4).

#### B. Numerical solution

The above equations have been solved by a multi-mode Galerkin method [15] that implies a full representation of the fields. In particular, it resolves the peculiar spatial structure in the concentration field [12, 13] in a sufficient way. Figure 1 shows the resulting bifurcation diagrams of TWs (full lines) and of SOC (dashed lines). The TW solution branch bifurcates at the Hopf bifurcation threshold  $r_{\text{osc}}$  with the Hopf frequency  $\omega_H$  out of the quiescent heat conducting

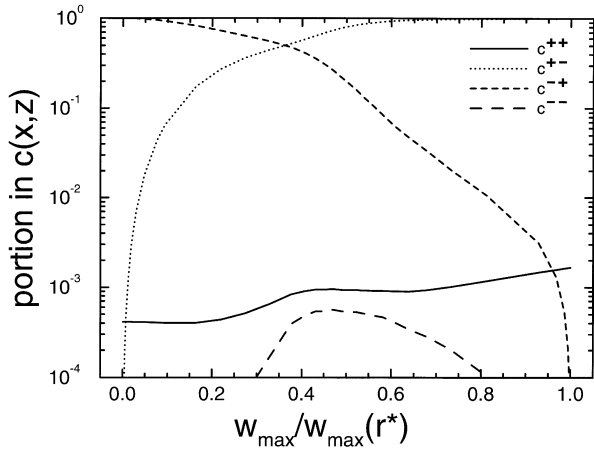


**Fig. 2.** The deviations  $c(x, z)$  of the concentration field from of its conductive profile are decomposed into four symmetry classes having definite parity under the operations  $x \rightarrow -x$  and  $z \rightarrow -z$ . The relative weight of the respective components  $c^{\pm\pm}$  in the complete field  $c(x, z)$  are plotted as a function of the maximal flow amplitude  $w_{\max}$  between the Hopf bifurcation ( $w_{\max} = 0$ ) and the SOC–TW–transition ( $w_{\max} = w_{\max}(r^*)$ ). Parameters are  $L = 0.01$ ,  $\sigma = 10$ , and  $\psi = -0.25$

state and it merges at  $r^*$  with the SOC branch. For these TWs we show in Fig. 2 how the different symmetry decomposed contributions to the TW concentration field  $c(x, z)$  vary as one moves along the TW bifurcation branch from  $w_{\max} = 0$ , i. e. the bifurcation out of the conductive state, to the end of the TW states at  $r^*$ . We measure the portion of a symmetry  $c^{\pm\pm}(x, z)$  in  $c(x, z)$  by  $\langle c^{\pm\pm}|c \rangle / \langle c^2 \rangle$  using global averaging as the scalar product. Thus,  $c(x, z)$  contains at  $r_{\text{osc}} (w_{\max} = 0)$  only contributions of the symmetries  $\mathcal{S}^{-+}$  (short dashed line) and  $\mathcal{S}^{++}$  (solid line). This reflects the fact that the critical eigenfunctions have positive vertical parity. However, already in weakly nonlinear states the portion of the symmetry  $\mathcal{S}^{+-}$  exceeds that of  $\mathcal{S}^{++}$  as a result of the strong increase of the zeroth lateral Fouriermode by the action of the convective nonlinearity. Near to the point where the TW phase velocity and the maximal convective velocity are equal and which has been identified [17] as the transition from weakly to strongly nonlinear TW convection the two symmetries  $\mathcal{S}^{+-}$  and  $\mathcal{S}^{-+}$  have the same portion in  $c(x, z)$ . Together, they make up 99.9% of it. Finally, at the SOC–TW–transition where the TW transforms into an SOC state there are no more contributions from  $\mathcal{S}^{-+}$  and  $\mathcal{S}^{--}$ .

A correct stability analysis of the conductive state needs test functions of the symmetries  $\mathcal{S}^{-+}$  and  $\mathcal{S}^{++}$  whereas the determination of the SOC–TW–transition which can be looked upon as a lateral parity breaking bifurcation of SOCs containing  $\mathcal{S}^{++}$  and  $\mathcal{S}^{+-}$  requires  $\mathcal{S}^{-+}$  and  $\mathcal{S}^{--}$ . Therefore, in principle all symmetries are necessary to describe the two transitions in the system in an adequate manner. The yet unmentioned symmetry  $\mathcal{S}^{--}$  (long dashed line in Fig. 2) contributes at most 0.06% of  $c(x, z)$  and is clearly the smallest portion in  $c(x, z)$  all over the bifurcation diagram. That is the reason why we think that modes of this symmetry — their influence will be discussed in Fig. 4 — are more or less irrelevant for the complex bifurcation scenario in convection of binary fluid mixtures.

## IV. Non–standard Galerkin approximation

### A. Mode selection

The simplest approach is to consider only one mode per symmetry class and to discard the  $\mathcal{S}^{--}$  part in the fields. This is the essence of older standard Galerkin approximations [14]. They yield linear relations between the square of the TW–frequency  $\omega$ , the square of the convection amplitude  $w_{\max}$  and the reduced Rayleigh number  $r = R/R_c^0$

$$\omega^2 = \alpha(r - r_{\text{osc}}) + \omega_{\text{H}}^2 \quad (4.1a)$$

$$w_{\max}^2 = \beta(r - r_{\text{osc}}) \quad (4.1b)$$

Here,  $\omega_{\text{H}}$  is the Hopf frequency at the oscillatory stability threshold  $r_{\text{osc}}$  of the basic state. These linear relations reproduce the onset of oscillatory convection and its weakly nonlinear properties in an adequate manner. However, they are not able to describe a saddle-node bifurcation and stable, strongly nonlinear TW convection. In fact, it was shown [18] that all Galerkin approximations using only one mode for each of the three symmetries  $\mathcal{S}^{++}$ ,  $\mathcal{S}^{-+}$ , and  $\mathcal{S}^{+-}$  yield linear relations like (4.1) — independent of the spatial shape of the modes.

Because of the smallness of the portion of  $\mathcal{S}^{--}$  in  $c(x, z)$  the simplest extension is to take *two* modes for each of the three relevant symmetries into account. This works reasonably well, as we will show below. Thus, such a model has to be looked upon as minimal model that is able to describe linear, weakly nonlinear, and strongly nonlinear states in binary fluid convection.

In order to provide adequate modes we use numerical solutions of the system as a basis for our non–standard Galerkin approximation. As one is interested in the description of an upper stable TW branch and the saddle-node bifurcation we symmetry decompose two states of the upper (numerically determined) TW branch and then orthonormalize them by a Gram–Schmidt–method using global averaging as scalar product.

For fluid parameters that are typically realized in mixtures of ethanol and water ( $L = 0.01$ ,  $\sigma = 10$ ,  $\psi = -0.25$ ) we use a fast TW near the saddle ( $\omega = 4$ ) and a slow one near the SOC–TW–transition ( $\omega = 0.125$ ). Both frequencies are small compared with the Hopf frequency of about 11.3. The resulting basis is displayed in Fig. 3. Since the structure of the temperature field changes only slightly along the whole bifurcation branch it is sufficient to consider only one temperature mode per symmetry. The three most important contributions to  $\theta$  are, like in the concentration field, the symmetries  $\mathcal{S}^{++}$ ,  $\mathcal{S}^{-+}$ , and  $\mathcal{S}^{+-}$ . Their contributions are very well described by the modes of the classical Lorenz model [19] and those of related approximations [14].

### B. Nonlinear stable TW states

Using the basis shown in Fig. 3 and the balance equations (2.3) one can derive a Galerkin model for convection in binary mixtures. This model has six or eight degrees of freedom for the description of the concentration field depending on whether the contribution of the symmetry  $\mathcal{S}^{--}$

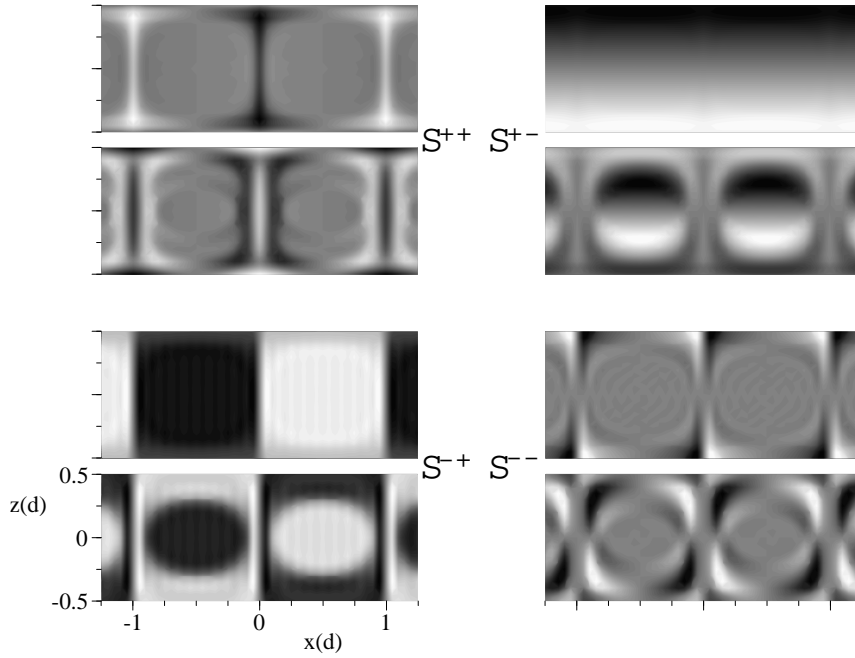


**Fig. 3.** Orthonormalized basis for the description of the concentration field in the  $x$ - $z$ -plane. The wave number is  $k = \pi$  so that the lateral periodicity length is 2. The four different symmetries are denoted by  $\mathcal{S}^{\pm\pm}$  at the side of the four blocks containing two basis elements each. The upper ones of each block are real states of the system ( $\omega = 0.125$ ) whereas the lower ones are linear combinations of two states resulting from the orthonormalization procedure

is contained or not. The temperature field is represented by three or four modes. As usual, projecting the field equations, e.g. (3.2), on the spatial modes of the respective fields yields a system of algebraic equations for the mode amplitudes. The order parameters of the velocity field,  $w_{\max}$  and  $\omega = vk$ , are computed from two algebraic equations for the velocity field that result after projection from (3.3). Here, we only want to discuss the bifurcation diagrams of the TWs, since those of the SOC are well enough reproduced by earlier approximations except for quantitative values of  $M$  and their stability properties.

Figure 4 shows from top to bottom the TW bifurcation diagrams of Nusselt number

$$N = \langle (\mathbf{u}T - \nabla T) \cdot \mathbf{e}_z \rangle_x |_{z=-1/2} = 1 - \langle \partial_z \theta \rangle_x |_{z=-1/2} ,$$

TW frequency  $\omega$ , and the reduced concentration variance

$$M = \sqrt{\frac{\langle C^2 \rangle}{\langle C_{cond}^2 \rangle}} = \frac{2\sqrt{3}}{|\psi|} \sqrt{\langle C^2 \rangle} .$$

These order parameters have been evaluated for extended models including  $\mathcal{S}^{--}$  modes (dotted lines) and neglecting them (dashed lines) in comparison with the “true” solution of the system (solid lines). The first thing to notice is that for a very good reproduction of the stable TW branch (the upper one in  $N$ , the lower ones in  $M$  and  $\omega$ ) the symmetry  $\mathcal{S}^{--}$  may not be neglected. Nevertheless,  $\mathcal{S}^{--}$  is not necessary for a qualitative correct bifurcation scenario of a Hopf bifurcation, a saddle-node bifurcation and a SOC–TW–transition on the stable, strongly nonlinear branch. This was not the case in earlier Galerkin models [14] connecting the basic state with the unstable SOC–branch by a TW–branch.

The positions of the SOC–TW–transitions given by the model including the  $\mathcal{S}^{--}$  symmetry and neglecting it differ as can be seen in Fig. 4. This can be explained as follows. This transition may be interpreted as a stability threshold of SOC whose lateral positive parity gets broken there. Since SOC contain both  $\mathcal{S}^{++}$  and  $\mathcal{S}^{+-}$  they need to be tested

for stability against disturbances of both  $\mathcal{S}^{+-}$  and  $\mathcal{S}^{--}$ . If one neglects  $\mathcal{S}^{--}$  the stability analysis is incomplete leading to different values for the threshold.

The correct bifurcation of the concentration variance  $M$  is due to an adequate description of the concentration field  $C(x, z)$  which is nearly 0 in SOC all over the convection cell except for small boundary layers between two adjacent rolls and at top and bottom plate so that the variance around its mean value is very small compared to the large concentration gradients in the basic state.

### C. Unstable TW solutions

The unstable TW branches resulting from the models differ from the exact ones [17], however without destroying the subcritical Hopf bifurcation topology — compare the dashed and dotted lower unstable branches of  $N$  up to the saddle in Fig. 4a with the full line (for  $\omega$  and  $M$  the upper branch corresponds to the unstable solution and is not shown in Fig. 4b and 4c). The reason for these differences is that the basic state is not tested for stability by the correct critical eigenfunctions. Since the oscillatory stability problem in binary fluid mixtures cannot be formulated as a variational principle as it is the case for the stationary one in a pure fluid [16] there is no need that an approximate stability threshold is higher than the exact one.

As mentioned already the position of the Hopf bifurcation does not depend on the presence of the symmetry  $\mathcal{S}^{--}$  since the basic state needs only to be tested for stability against disturbances of the symmetries  $\mathcal{S}^{++}$  and  $\mathcal{S}^{+-}$ . However, the initial slope of, e. g., the Nusselt number  $N$  being a nonlinear property involves modes of the symmetry  $\mathcal{S}^{--}$  that are driven by the critical modes with the symmetries  $\mathcal{S}^{++}$  and  $\mathcal{S}^{+-}$  via the convective nonlinearity. All this can be seen in Fig. 4a where the dotted and dashed lines have a common bifurcation threshold out of the basic state ( $N = 1$ ) but spread in the nonlinear regime ( $N > 1$ ). A

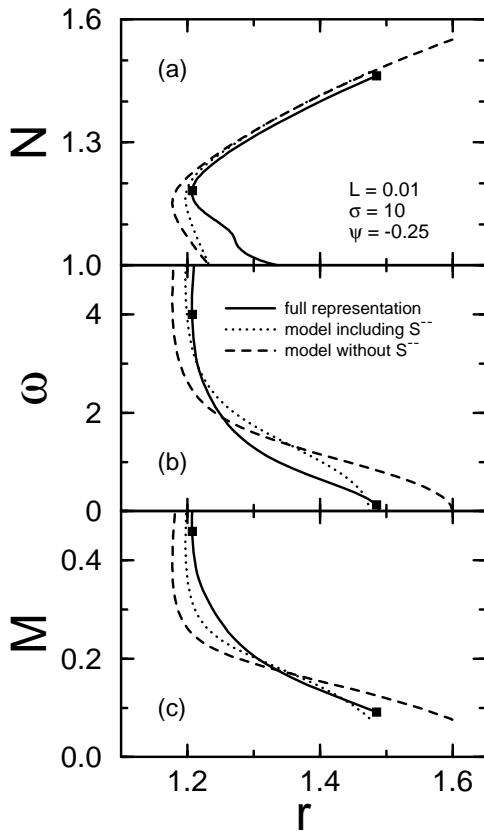


**Fig. 4.** Bifurcation diagrams of Nusselt number  $N$  **a**, TW frequency  $\omega$  **b** and concentration variance  $M$  **c** in the framework of Galerkin models with numerical basis including the symmetry  $\mathcal{S}^-$  (dotted line) or discarding it (dashed line) in comparison with results of a many mode analysis (solid line). The filled squares show the two states which were used to construct a basis for the models. Parameters are  $L = 0.01$ ,  $\sigma = 10$ ,  $\psi = -0.25$ , and  $k = \pi$

qualitatively better reproduction of the unstable TW branch is obtained by changing the basis of the Galerkin model, namely by using states of the correct unstable TW branch. Then, the approximation quality of the stable states which are the main topic of this work deteriorates.

#### D. Dependence on the separation ratio $\psi$

Numerical simulations [13] have shown that the concentration distribution depends only slightly on the separation ratio  $\psi$  for the small Lewis numbers  $L = O(0.01)$  and large Prandtl numbers  $\sigma = O(10)$  that are typically realized in mixtures of ethanol and water. This insensitiveness of the concentration field towards changes in  $\psi$  suggests that our above presented models also describe convection in binary mixtures with values of  $\psi$  different to those where the basis is extracted.

The changes in the bifurcation topology caused by varying the strength  $\psi$  of the Soret coupling may be described by tracing out the  $\psi$ -dependences of the SOC and TW saddle-node bifurcations  $r_{\text{SOC}}^s$  and  $r_{\text{TW}}^s$ , and of the SOC–TW–transition  $r^*$ . This is shown in Fig. 5 for the model containing all symmetries (lines) in comparison with the full representation of the fields (symbols). Both saddles of the

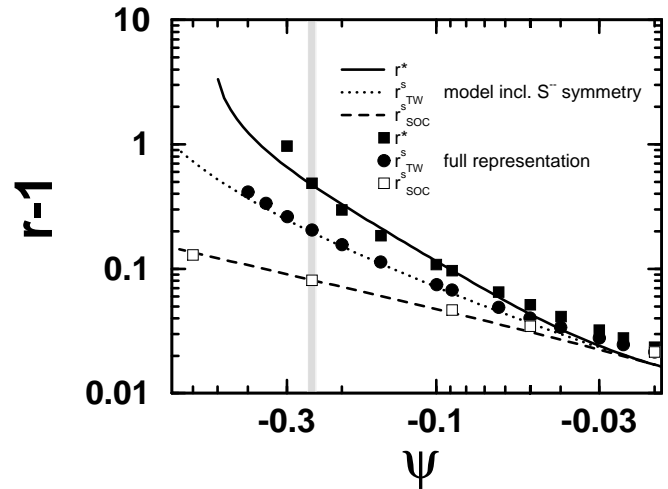


**Fig. 5.** Phase diagrams of the here presented non–standard Galerkin model (lines) in comparison with the results of a full representation (symbols). The basis of the model was fixed at  $\psi = -0.25$  as indicated by the grey bar. The  $\psi$ -dependence of the SOC–TW–transition  $r^*$  (solid line, filled squares), the TW saddle-node bifurcation  $r_{\text{TW}}^s$  (dotted line, filled circles), and the saddle-node bifurcation of the SOC branch  $r_{\text{SOC}}^s$  (dashed line, open squares) is shown in a double logarithmical plot. Parameters are  $L = 0.01$  and  $\sigma = 10$

SOC and TW bifurcation diagrams procured by our non–standard model are in good quantitative agreement with the results of the full representation. The model only deviates for weak Soret couplings  $\psi > -0.04$ . This can be explained by the smoother variations of the concentration field for those couplings (see e. g. [13]). The same holds for the SOC–TW–transition  $r^*$  which in addition differs for strong Soret couplings  $\psi < -0.3$ . This is due to the fact that the SOC–TW–transition can be interpreted as a boundary layer instability [20] which therefore is very sensitive to the thickness of the boundary layers in the concentration field. However, the thickness of the boundary layer is fixed in a model with fixed modes. Nevertheless, the model is able to describe the  $\psi$ -dependence of both TW– and SOC–bifurcation scenario quite well.

#### V. Conclusion

In this article we have presented a model describing traveling wave convection in binary fluid mixtures. Their complex bifurcation scenario is reproduced by a Galerkin method using two numerically obtained exact solutions of the system as a basis. These solutions for fixed fluid parameters are symmetry decomposed in order to meet the symmetry properties of the bifurcations and of the states in the system. We have shown that there exists a minimal number of degrees of freedom for the description of the concentration field. Our model uses this minimal number and reproduces numerically and experimentally observed states in binary fluid mixtures very well. In addition, it describes the dependence of the bifurcation topology on the strength of the Soret coupling quite well. Furthermore, it shows that in the temperature and velocity field the modes of the classical Lorenz model [19] are sufficient. Finally, the model gives useful hints for

a derivation of an approximation using analytical test functions instead of the here applied numerical ones.

This work was supported by Deutsche Forschungsgemeinschaft. Discussions with W. Barten, P. Büchel, and H. W. Müller are gratefully acknowledged as well as a graduate scholarship of the Saarland for one of us (SH).

## References

1. M. C. Cross, P. C. Hohenberg: *Rev. Mod. Phys.* **65**, 851 (1993)
2. J. K. Platten, J. C. Legros: Berlin: Springer 1984
3. R. W. Walden, P. Kolodner, A. Passner, C. M. Surko: *Phys. Rev. Lett.* **55**, 496 (1985)
4. H. Touiri, J. K. Platten, G. Chavepeyer: *Eur. J. Mech., B/Fluids* **15**, (2) 241, (1996)
5. G. Ahlers, I. Rehberg: *Phys. Rev. Lett.* **56**, 1373 (1986)
6. H. Gao, R. P. Behringer: *Phys. Rev.* **A34**, 697 (1986)
7. E. Moses, V. Steinberg: *Phys. Rev. Lett.* **60**, 2030 (1988)
8. K. D. Eaton, D. R. Ohlsen, S. Y. Yamamoto, C. M. Surko, W. Barten, M. Lücke, M. Kamps, P. Kolodner: *Phys. Rev.* **A43**, 7105 (1991)
9. G. Zimmermann, U. Müller: *Int. J. Heat Mass Transfer* **35**, 2245 (1992)
10. B. L. Winkler, P. Kolodner: *J. Fluid Mech.* **240**, 31 (1992)
11. A. La Porta, K. D. Eaton, C. M. Surko: *Phys. Rev.* **E53**, 570 (1996)
12. W. Barten, M. Lücke, W. Hort, M. Kamps: *Phys. Rev. Lett.* **63**, 376 (1989); W. Barten, M. Lücke, M. Kamps, In: *Nonlinear Evolution of Spatio-Temporal Structures in Dissipative Continuous Systems*, NATO ASI Series **B225**, p. 131 New York: Plenum Press 1990
13. W. Barten, M. Lücke, M. Kamps, R. Schmitz: *Phys. Rev.* **E51**, 5636 (1995)
14. S. J. Linz, M. Lücke, H. W. Müller, J. Niederländer: *Phys. Rev.* **A38**, 5727 (1988); O. Lhost: *Etude de la Convection Libre Induite par effet Soret*, Thesis, Mons (1990, unpublished)
15. St. Hollinger, M. Lücke: unpublished
16. S. Chandrasekhar: *Hydrodynamic and Hydromagnetic Stability*, New York: Dover 1981
17. St. Hollinger, P. Büchel, M. Lücke: *Phys. Rev. Lett.* **78**, 235 (1997)
18. St. Hollinger: *Einfluß des Dufoureffekts auf die Konvektion in binären Gasmischungen*, Diplomarbeit, Saarbrücken (1993, unpublished)
19. E. N. Lorenz: *J. Atmospheric Sciences* **20**, 130 (1963); J. Niederländer, M. Lücke, M. Kamps: *Z. Phys.* **B82**, 135 (1991)
20. D. Bensimon, A. Pumir, B. I. Shraiman: *J. Phys. (France)* **50**, 3089 (1989)